

RESEARCH ARTICLE

Open Access



Differentiation of suprasellar meningiomas from non-functioning pituitary macroadenomas by ^{18}F -FDG and ^{13}N -Ammonia PET/CT

Lei Ding^{1†}, Fangling Zhang^{1,2†}, Qiao He¹, Zhoulei Li¹, Xinchong Shi¹, Ruocheng Li¹ and Xiangsong Zhang^{1*}

Abstract

Background: Differentiation of suprasellar meningiomas (SSMs) from non-functioning pituitary macroadenomas (NFPMA) is useful for clinical management. We investigated the utility of ^{13}N -ammonia combined with ^{18}F -FDG positron emission tomography (PET)/computed tomography (CT) in distinguishing SSMs from NFPMA retrospectively.

Methods: Fourteen NFPMA patients and eleven SSM patients with histopathologic diagnosis were included in this study. Every patient underwent both ^{18}F -FDG and ^{13}N -ammonia PET/CT scans. The tumor to gray matter (T/G) ratios were calculated for the evaluation of tumor uptake.

Results: The uptake of ^{18}F -FDG was higher in NFPMA than SSMs, whereas the uptake of ^{13}N -ammonia was obviously lower in NFPMA than SSMs. The differences of ^{18}F -FDG and ^{13}N -ammonia uptake between the two groups were significant respectively (0.92[0.46] vs 0.59[0.29], $P < 0.05$, ^{18}F -FDG; 1.58 ± 0.56 vs 2.80 ± 1.45 , $P < 0.05$, ^{13}N -ammonia). Tumor classification demonstrated a high overall accuracy of 96.0% for differential diagnosis. When the two traces were combined, only 1 SSM was misclassified into the NFPMA group.

Conclusion: SSMs and NFPMA have different metabolic characteristics on ^{18}F -FDG and ^{13}N -ammonia PET images. The combination of these two tracers can effectively distinguish SSMs from NFPMA.

Keywords: Non-functioning pituitary macroadenoma, Suprasellar meningioma; ^{18}F -FDG; ^{13}N -ammonia; PET-CT

Background

SSMs have been classified into three subtypes according to the original site and central location of the tumors: tuberculum sellae, planum sphenoidale and diaphragm sellae meningiomas [1–3]. The wide operative field of the trans-cranial approach is more appropriate for these firm tumors [2, 4]. Pituitary adenomas are the most

common sellar region tumors and the surgery are conducted usually with the trans-sphenoidal approach [5]. SSMs can mimic other non-hormone secreting sellar region masses both clinically and radiologically, in particular the NFPMA. In neurosurgical practice, it is important to distinguish SSMs from NFPMA, which can result in differences in surgery program. Magnetic resonance imaging (MRI) is the most common neuroimaging modality owing to its excellent soft-tissue contrast and spatial resolution at present. In comparison with moderate and heterogeneous enhancement of NFPMA, previous studies stated marked and homogeneous

* Correspondence: flyzfl@126.com

[†]Lei Ding and Fangling Zhang contributed equally to this work.

¹Department of the Medical Imaging, The First Affiliated Hospital, Sun Yat-sen University, 58# Zhongshan Er Road, Guangzhou, Guangdong Province 510080, People's Republic of China

Full list of author information is available at the end of the article



© The Author(s). 2020 **Open Access** This article is licensed under a Creative Commons Attribution 4.0 International License, which permits use, sharing, adaptation, distribution and reproduction in any medium or format, as long as you give appropriate credit to the original author(s) and the source, provide a link to the Creative Commons licence, and indicate if changes were made. The images or other third party material in this article are included in the article's Creative Commons licence, unless indicated otherwise in a credit line to the material. If material is not included in the article's Creative Commons licence and your intended use is not permitted by statutory regulation or exceeds the permitted use, you will need to obtain permission directly from the copyright holder. To view a copy of this licence, visit <http://creativecommons.org/licenses/by/4.0/>. The Creative Commons Public Domain Dedication waiver (<http://creativecommons.org/publicdomain/zero/1.0/>) applies to the data made available in this article, unless otherwise stated in a credit line to the data.

enhancement and “dural tail” sign with contrast as unique characteristics of SSMs [6, 7]. Moreover, mostly suprasellar center, moderate sella turcica enlargement and separation from pituitary gland may also be diagnostic elements for SSMs [8]. Nevertheless, accurate pre-operative diagnosis is still quite challenging and difficult by current morphological imaging modalities alone because of the overlap of imaging findings and the relatively rarity of SSMs. MRI should be complemented by PET in whether diagnosis and staging before treatment or postoperative therapeutic effectiveness monitoring [9]. ^{13}N -ammonia is suggested to be a contrast-enhanced radiotracer which is more sensitive and specific than Gadolinium-Diethylenetriaminepentaacetic acid (Gd-DTPA) [10]. We have reported the clinical usefulness of ^{13}N -ammonia in many brain tumors through a series of studies [11–14]. In addition, ^{13}N -ammonia is also a potential tracer targeting glutamine synthetase (GS) expression which is associated with ammonia-glutamine synthesis reaction [15]. In this study, we aimed to investigate the combined efficiency of ^{18}F -FDG and ^{13}N -ammonia PET/CT in distinguishing SSMs from NFPMA.

Methods

Patient

SSMs which broke through the diaphragma sellae and grew into the pituitary fossa and more than 1 cm in diameter, NFPMA which grew anteriorly and superiorly and more than 1 cm in diameter were included in our study. Eventually the data of 25 patients in our center were enrolled in the study between July 2009 to December 2018. 14 patients with NFPMA (7 female and 7 male; mean age, 47.81 ± 10.04 years; range, 37–68 years) and 11 patients with SSM (9 female and 2 male; mean age, 55.69 ± 14.37 years; range, 41–83 years). All patients were absent of any therapeutic interventions before imaging examination and underwent PET/CT scan with ^{18}F -FDG and ^{13}N -ammonia within 5 days. Histopathological diagnosis was obtained after PET/CT scan for all cases. This study was approved by the hospital ethics committee. Detailed study purpose and imaging procedure were explained to every patient, and the need for signed informed consent was waived.

PET/CT imaging

PET/CT scan was performed with a Gemini GXL-16 scanner (Philips, Netherlands) in 3-dimensional acquisition mode. ^{18}F -FDG and ^{13}N -ammonia were produced in our center using standard techniques and commercially available systems for isotope generation (Ion Beam Applications, Cyclone-10, Belgium). PET images were acquired by a particular imaging protocol for the brain with a field of view of 180 mm, reconstructed by the line of response algorithm and attenuation-corrected using

low-dose CT. All patients fasted for at least eight hours and urinated just before PET/CT scan. About Forty-five minutes after an intravenous injection of ^{18}F -FDG (5.18 MBq/kg) and five minutes after an intravenous injection of ^{13}N -ammonia (370–740 MBq), a 10-min PET/CT scan started. ^{18}F -FDG and ^{13}N -ammonia studies were performed at least 24 h apart.

Imaging analysis

Visual analysis

For visual analysis, the degree of tracer uptake by the lesion was visually classified into 3 grades compared with the contralateral or surrounding normal brain parenchyma: high metabolism, moderate metabolism and low metabolism.

Semiquantitative analysis

The uptake of the tumor was evaluated using the maximum standard uptake value (SUV_{max}). For each patient, a region of interest (ROI) with 10 mm in diameter was drawn in the area of highest activity within the tumor in trans-axial plane. Then another reference ROI was placed on the normal contralateral gray matter of pre-frontal cortex. The SUV_{max} of all ROIs were used for the calculation of T/G ratios. MRI images were referred to avoid the area of necrosis or hemorrhage by coregistering PET and MR images with the software of MIPAV (Center for Information Technology, National Institutes of Health, Maryland), especially in cases without significant tracer concentration.

Statistical analysis

Statistical analysis was processed with SPSS 20.0 software (<http://www.ibm.com>). Result was considered statistically significant when the P value was less than 0.05. In this study, Student t test was firstly applied to compare the T/G ratios between NFPMA group and SSM group for each tracer. Then the T/G ratios of both tracers were used as multiple variables for the discrimination analysis of the two groups, generating the canonical discriminant function. As a result, each patient was classified into one group successfully according to the function result and cross validation was done to assess the differential usefulness when the two traces were combined.

Results

All of the SSMs in our study are grade I referring to the 2016 World Health Organization (WHO) classification, including 7 meningothelial meningiomas, 3 transitional meningiomas and 1 fibrous meningioma histopathologically. The diameter of NFPMA and SSMs ranged from 1.2 to 5.8 cm (mean \pm SD, 3.08 ± 1.25 cm) and 2.4 to 7.6 cm (mean \pm SD, 3.37 ± 1.58 cm) respectively.

For NFPMAs, there were 2(14.3%), 8(57.1%), 4(28.6%) of the 14 cases showed low, moderate and high metabolism respectively on ^{18}F -FDG images and 3(21.4%), 8(57.1%), 3(21.4%) of the 14 cases showed low, moderate and high metabolism respectively on ^{13}N -ammonia images. For SSMs, there were 7(63.6%), 4(36.4%) of the 11 cases showed low and moderate metabolism respectively on ^{18}F -FDG images and 11(100%) of the 11 cases showed high metabolism on ^{13}N -ammonia images.

The uptake results were shown in Fig. 1. There were significant differences of ^{18}F -FDG and ^{13}N -ammonia uptake between the two clinical entities. The uptake of ^{18}F -FDG was higher in NFPMAs than SSMs ($0.92[0.46]$ vs $0.59[0.29]$, $P < 0.05$), whereas the concentration of ^{13}N -ammonia was lower in NFPMAs than SSMs (1.58 ± 0.56 vs 2.80 ± 1.45 , $P < 0.05$) (Fig. 2). Tumor classification by canonical discriminant analysis with T/G values of both tracers showed the optimal discriminant function was $F(x, y) = -2.191x + 0.946y - 0.473$, where x represented T/G ratio of ^{18}F -FDG and y represented T/G ratio of ^{13}N -ammonia. Therefore, the function result of NFPMAs was -1.23 ± 0.96 , which was significantly lower than that of SSMs (1.57 ± 1.01 , $P < 0.001$). The predicted accuracy for NFPMAs and SSMs was 100 and 90.9% respectively. Only 1 SSM was misdiagnosed as NFPMA and the overall diagnostic accuracy was 96.0% (Table 1, Fig. 3).

Discussion

NFPMAs can cause hypopituitarism and hyperprolactinemia or even show no endocrinologic abnormalities, which is similar to SSMs [16]. Headaches, loss of visual acuity and visual field are some other common symptoms for these patients [7, 17]. Most intra-suprasellar adenomas are excised via the trans-sphenoidal route to our knowledge [18]. Unlike the soft pituitary adenomas, SSMs are highly vascular, firm and adhesive to adjacent neurovascular structures [19]. A transcranial approach is commonly considered for most SSMs, which can achieve a high rate of total resection with a low rate of postoperative cerebrospinal fluid leak, hemorrhage and nerve injury [4, 20, 21]. SSMs are sometimes amenable to resection by trans-sphenoidal route and some authors advocated that this approach can result in comparable outcomes with trans-cranial approach in carefully and critically selected patients [22, 23]. Generally speaking, the determination of an optimum surgical approach depends on multiple factors, such as tumor size, consistency, location, relationships with the adjacent structures and the presenting symptoms [24]. Therefore, surgical plan could be implemented more effectively and safely if an accurate pre-operative diagnosis is available.

MRI has played an irreplaceable role in the diagnosis of sellar and suprasellar tumors for a long time and most

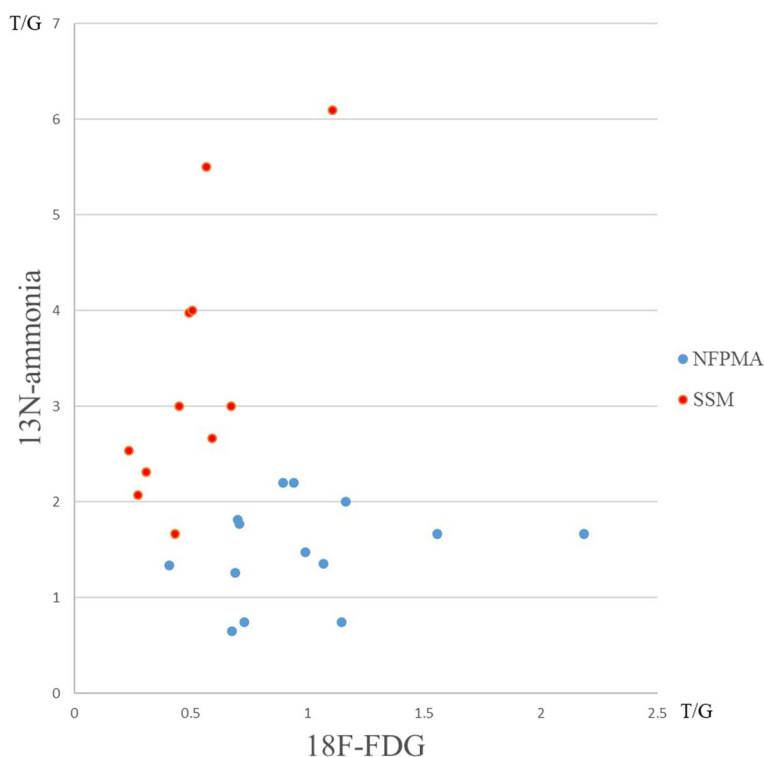
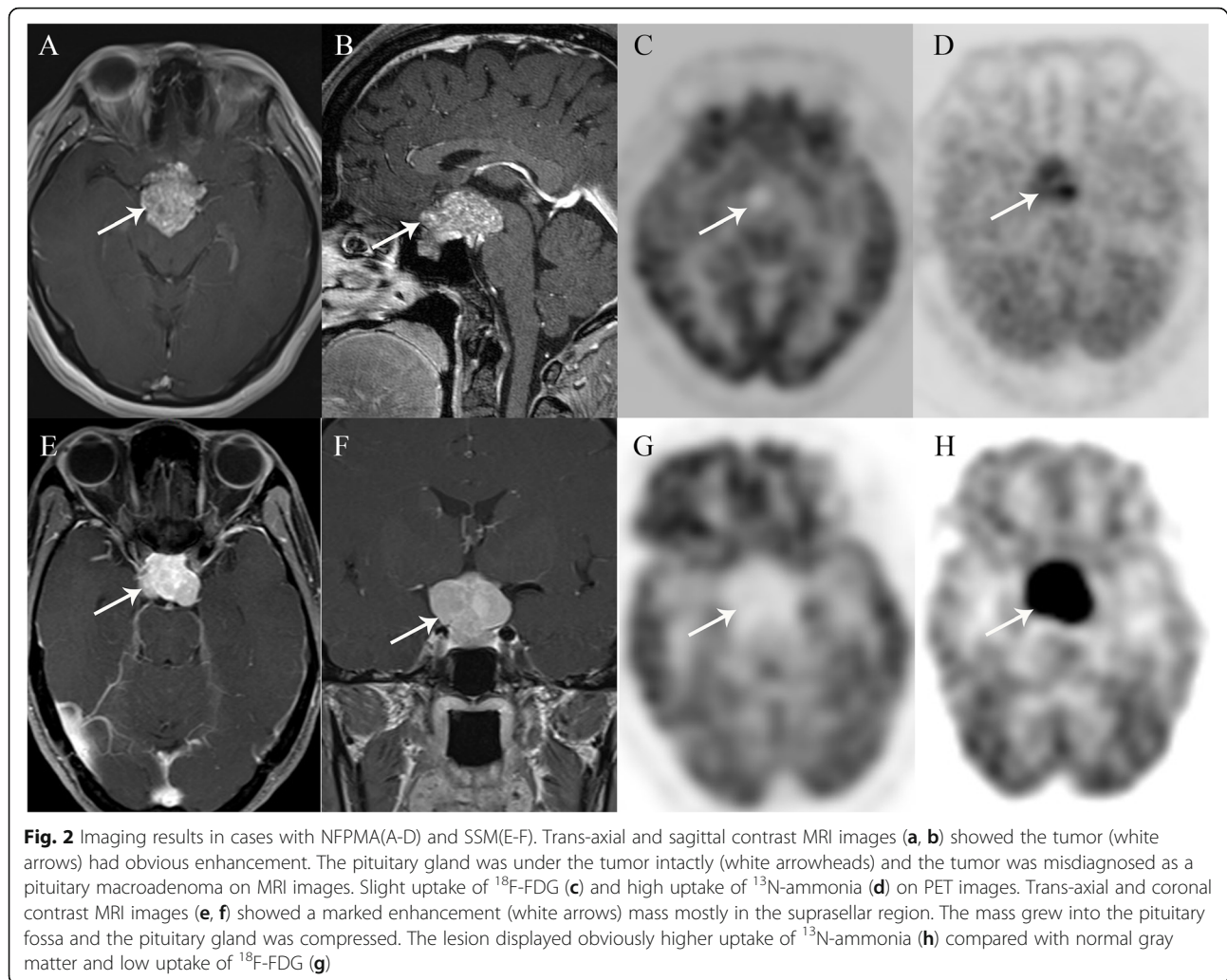


Fig. 1 Distribution map of T/G ratios of ^{18}F -FDG and ^{13}N -ammonia. As shown in this figure, there was a small overlap between NFPMA (blue spot) and SSM (red spot)



SSMs can be differentiated from NAPMAs based on it. Sometimes SSMs can break through the diaphragma sellae and grow into the pituitary fossa, making it similar to NFPMAs extending anteriorly and superiorly on conventional morphological imaging [7, 25]. Magnetic resonance brain functional imaging methods such as perfusion-weighted imaging (PWI) can be valuable for brain tumors by detecting the hemodynamic state. However, PWI is not always used in an efficient way. Firstly,

PWI is highly user-dependent because the accurate recognition of blood vessels is challenging and the standardization is lacking in data processing methods presently. Besides, PWI is difficult to implemented in regions close to a brain–bone–air interface such as the skull base [26–28]. As one of the most important molecular imaging modalities, PET should be considered as complementary tools in the evaluation of brain tumors and PET even seems to show a more significant role than such MR advanced techniques [28, 29]. ^{18}F -FDG is the most common PET/CT tracer and the molecular mechanism has been clarified previously [30]. However, the inherent limitation of high physiologic uptake in the normal brain tissue necessitates the search for other newer PET tracers. Although ^{13}N -ammonia has a short half-life time, it is rapidly spreading in recent years because of its diagnostic power (perfusion-metabolism coupling tracer) and the easier interpretation for clinicians owing to the higher tumor to back-ground contrast compared to PWI and other PET tracers [31]. On the

Table 1 Predicted accuracy of discriminant analysis for the 2 groups

	n (%)	Predicted Group Membership	Group		Total
			NFPMA	SSM	
Original	n (%)	NFPMA	14 (100)		14 (100)
		SSM	1 (9.1)	10 (90.9)	11 (100)
Cross-validated	n (%)	NFPMA	14 (100)		14 (100)
		SSM	1 (9.1)	10 (90.9)	11 (100)

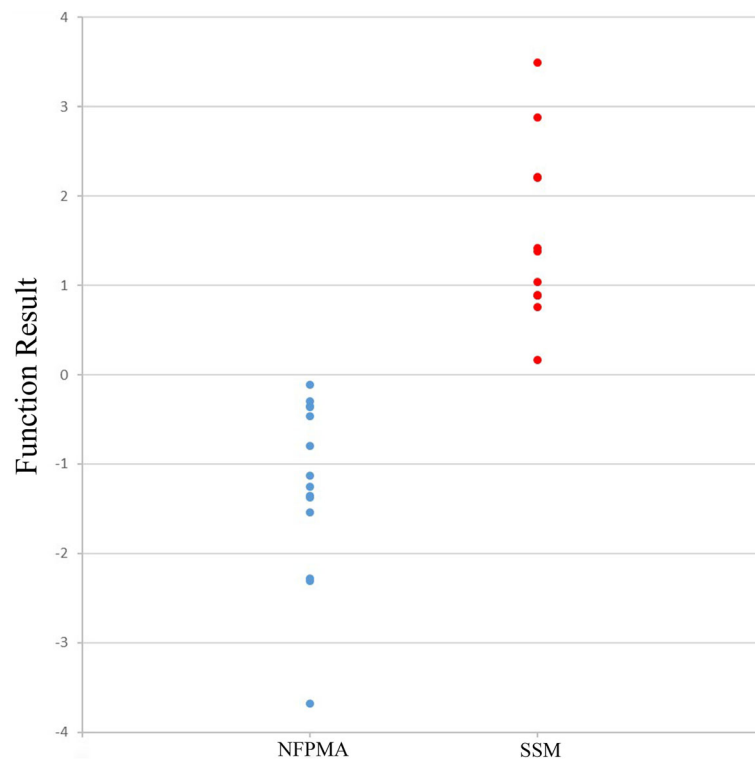


Fig. 3 Discriminant function results of T/G ratios between the two groups. The function results of NFPMA were obviously lower than that of SSM (-1.23 ± 0.96 vs 1.57 ± 1.01). The combination of the two tracers could distinguish these two clinical entities effectively

other hand, the short half-life time has the advantage of reducing the radiation. Actually, the synthesis time for ^{13}N -ammonia is short and the process is convenient by the cyclotron. According to previous studies of our department, ^{13}N -ammonia has potential diagnostic value in brain tumor [10, 11, 32, 33].

In our study, SSMs showed a higher uptake than NFPMAs on ^{13}N -ammonia PET images. In contrast, NFPMAs showed a higher uptake than SSMs on ^{18}F -FDG PET images. All SSMs are grade I, demonstrating lower glucose consumption than normal gray matter. The normal pituitary gland showed little uptake because of its small size and low metabolic rate on ^{18}F -FDG PET images. On the other hand, pituitary adenomas were more metabolically active than normal pituitary gland and SSMs and the uptake was related to the size of the adenomas [34, 35]. ^{18}F -FDG PET/CT was useful for detecting NFPMAs [36, 37]. For ^{13}N -ammonia, we found it had great value in the diagnosis of SSMs. ^{13}N -ammonia is lipid soluble and has small molecular weight (16 Da) compared to Gd-DTPA (approximately 470 Da) [38]. The blood ammonia mainly exists in two forms at physiological blood pH, that is unionized ammonia (NH_3 , about 3%) and ionized species (NH_4^+ , about 97%). Compared with ionized form. The unionized form can pass the blood brain barrier (BBB) freely and be

rapidly supplemented from the ionized form since the two forms are in equilibrium through the reaction $\text{NH}_4^+ \leftrightarrow \text{NH}_3 + \text{H}^+$ [39–41]. Actually, the initial extraction of ^{13}N -ammonia depends on the cerebral blood flow (CBF) and capillary permeability-surface (PS) area product [42]. As glutamine contributes to the production of adenosine triphosphate (ATP), the biosynthesis of macromolecules and the modulation of redox homeostasis, it is important for the survival of tumor cells [43]. Tumor cells can not only obtain glutamine from plasma but also can synthesize glutamine by themselves intracellularly. GS is the only enzyme known which can convert ammonia and glutamate to glutamine in the mammalian brain tissue [39]. Since the up-regulation of GS is widely interpreted as a reflection of active glutamine metabolism and the up-regulation has been reported in many tumors [42, 44–46], the expression of GS is another factor contributing to the ^{13}N -ammonia trapping, that is, metabolic trapping [47–49]. In our study, meningiomas exhibited extremely high accumulation of ^{13}N -ammonia against the surrounding tissue because of the absence of BBB, increased regional CBF coupled with increased PS (due to neovascularization), indicating that ^{13}N -ammonia is an ideal tracer to identify meningiomas. Immunohistochemical staining of brain tumor biopsies indicated that the GS activity of meningiomas was strongly

positive and the expression was not limited to any particular histopathological variants. Amongst the tumors the highest levels were found in the astrocytoma and oligodendroglioma and GS level was higher in meningiomas than pituitary adenomas [39, 46]. Similarly, the normal pituitary tissue clearly showed obviously high uptake of ^{13}N -ammonia. Previous study also demonstrated that GS activity was present in the anterior pituitary gland [50]. Since ^{13}N -ammonia PET/CT imaging is valuable in detecting pituitary tissue, surgeons can carefully find the pituitary tissue guided by PET so that maximize the protection of the pituitary tissue. This is another reason for the use of ^{13}N -ammonia in the sellar region tumors [51]. For NFPMA, relatively poor neovascularization compared with SSMs and normal pituitary tissue was confirmed on contrast CT and MRI imaging, providing a limited amount of radiotracer for trapping. From the visual results, we found there were uptake overlap between NFPMA and SSMs for each tracer. The combination of ^{18}F -FDG and ^{13}N -Ammonia PET/CT could derive a more favorable results for increasing the accuracy to the maximum.

Our study yielded significant results and proposed a new viewpoint for the prediction of SSMs. However, it was inevitable that there were several limitations. Firstly, we collected a small sample of SSMs, and the research results need further confirmation by prospective studies with larger sample capacity. In addition, ^{13}N -ammonia has a very short half-life time (9.965 min), so a cyclotron onsite is required for clinical application. Lastly, we failed to detect the GS expression in meningioma specimens limited to the access to resources.

Conclusion

SSMs and NFPMA have different metabolic characteristics on ^{18}F -FDG and ^{13}N -ammonia PET images. The combination of these two tracers can effectively distinguish SSMs from NFPMA.

Abbreviations

SSMs: Suprasellar meningiomas; NFPMA: Non-functioning pituitary macroadenomas; PET: Positron emission tomography; CT: Computed tomography; T/G: Tumor to normal gray matter; MRI: Magnetic resonance imaging; Gd-DTPA: Gadolinium-Diethylenetriaminepentaacetic acid; GS: Glutamine synthetase; SUV_{max} : Maximum standard uptake value; ROI: Region of interest; PWI: Perfusion-weighted imaging; BBB: Blood brain barrier; CBF: Cerebral blood flow; PS: Permeability-surface; GS: Glutamine synthetase; ATP: Adenosine triphosphate

Acknowledgements

We would like to thank all members of the Drug Synthesis Department for the preparation of PET tracers, and all nuclear technologists for image collecting and processing in PET/CT center.

Authors' contributions

LD and FLZ participated in the design of the study, collected the patients' data, and drafted the manuscript. QH, ZLL, XCS and RCL processed the figures, helped draft the manuscript, and performed a critical revision of

the manuscript. XSZ conceived and designed the study and supervised the project. All authors read and approved the final version of the manuscript.

Funding

This work was supported by the National Natural Science Foundation of China (No.81501509 to XSZ), the Science and Technology Planning Projects of Guangdong Province (No: 2017B020210001 to XSZ) and the Training Program of the Major Research Plan of Sun Yat-Sen University (No:17ykjc10 to XSZ). Funding supporter played no role in the design of the study and collection, analysis, and interpretation of data and in writing the manuscript.

Availability of data and materials

The dataset supporting the conclusions of this article is included within the article. Data and materials during the current study are available from the corresponding author upon reasonable request.

Ethics approval and consent to participate

The current study was approved by the Institutional Ethics Committee of the First Affiliated Hospital of Sun Yat-Sen University, and the need for signed informed consent was waived.

Consent for publication

Not applicable.

Competing interests

The authors declare that they have no competing interests.

Author details

¹Department of the Medical Imaging, The First Affiliated Hospital, Sun Yat-sen University, 58# Zhongshan Er Road, Guangzhou, Guangdong Province 510080, People's Republic of China. ²Department of Radiology, Hospital of Stomatology, Guanghua School of Stomatology, Sun Yat-sen University; Guangdong Provincial Key Laboratory of Stomatology, 56#, Cemetery west Road, Guangzhou, Guangdong Province 510055, People's Republic of China.

Received: 29 August 2019 Accepted: 12 April 2020

Published online: 17 June 2020

References

- Wang CW, Li YY, Zhu SG, et al. Surgical management and evaluation of prognostic factors influencing postoperative visual outcome of suprasellar meningiomas. *World Neurosurg.* 2011;75(2):294–302.
- Komotar RJ, Starke RM, Raper DM, Anand VK, Schwartz TH. Endoscopic endonasal versus open transcranial resection of anterior midline skull base meningiomas. *World Neurosurg.* 2012;77(5–6):713–24.
- Ajlan AM, Choudhri O, Hwang P, Harsh G. Meningiomas of the tuberculum and diaphragma sellae. *J Neurol Surg B Skull Base.* 2015;76(1):74–9.
- Nanda A, Ambekar S, Javalkar V, Sharma M. Technical nuances in the management of tuberculum sellae and diaphragma sellae meningiomas. *Neurosurg Focus.* 2013;35(6):E7.
- Shen CC, Wang YC, Hua WS, Chang CS, Sun MH. Endoscopic endonasal transsphenoidal surgery for pituitary tumors. *Zhonghua Yi Xue Za Zhi (Taipei).* 2000;63(4):301–10.
- Cappabianca P, Cirillo S, Alfieri A, et al. Pituitary macroadenoma and diaphragma sellae meningioma: differential diagnosis on MRI. *Neuroradiology.* 1999;41(1):22–6.
- Kwancharoen R, Blitz AM, Tavares F, Caturegli P, Gallia GL, Salvatori R. Clinical features of sellar and suprasellar meningiomas. *Pituitary.* 2014;17(4):342–8.
- Donovan JL, Nesbit GM. Distinction of masses involving the Sella and suprasellar space: specificity of imaging features. *AJR Am J Roentgenol.* 1996;167(3):597–603.
- Singhal T. Positron emission tomography applications in clinical neurology. *Semin Neurol.* 2012;32(4):421–31.
- Xiangsong Z, Xinjian W, Yong Z, Weian C. ^{13}N -NH₃: a selective contrast-enhancing tracer for brain tumor. *Nucl Med Commun.* 2008;29(12):1052–8.
- Xiangsong Z, Weian C, Dianchao Y, Xiaoyan W, Zhifeng C, Xiongchong S. Usefulness of ^{13}N -NH₃ PET in the evaluation of brain lesions that are hypometabolic on ^{18}F -FDG PET. *J Neuro-Oncol.* 2011;105(1):103–7.

12. Shi X, Liu Y, Zhang X, et al. The comparison of 13N-ammonia and 18F-FDG in the evaluation of untreated gliomas. *Clin Nucl Med*. 2013;38(7):522–6.
13. Shi X, Yi C, Wang X, et al. 13N-ammonia combined with 18F-FDG could discriminate between necrotic high-grade gliomas and brain abscess. *Clin Nucl Med*. 2015;40(3):195–9.
14. Xiangsong Z, Xingchong S, Chang Y, Xiaoyan W, Zhifeng C. 13N-NH3 versus F-18 FDG in detection of intracranial meningioma: initial report. *Clin Nucl Med*. 2011;36(11):1003–6.
15. Yamamoto H, Konno H, Yamamoto T, Ito K, Mizugaki M, Iwasaki Y. Glutamine synthetase of the human brain: purification and characterization. *J Neurochem*. 1987;49(2):603–9.
16. Zaidi HA, Cote DJ, Castlen JP, et al. Time course of resolution of Hyperprolactinemia after Transphenoidal surgery among patients presenting with pituitary stalk compression. *World Neurosurg*. 2017;97:2–7.
17. Castlen JP, Cote DJ, Zaidi HA, Laws ER Jr. The extended, transnasal, transphenoidal approach for anterior skull base meningioma: considerations in patient selection. *Pituitary*. 2017;20(5):561–8.
18. Kawamata T, Iseki H, Shibasaki T, Hori T. Endoscopic augmented reality navigation system for endonasal transphenoidal surgery to treat pituitary tumors: technical note. *Neurosurgery*. 2002;50(6):1393–7.
19. Koutourousiou M, Fernandez-Miranda JC, Wang EW, Snyderman CH, Gardner PA. Endoscopic endonasal surgery for olfactory groove meningiomas: outcomes and limitations in 50 patients. *Neurosurg Focus*. 2014;37(4):E8.
20. Morales-Valero SF, Van Gompel JJ, Loumiotis I, Lanzino G. Craniotomy for anterior cranial fossa meningiomas: historical overview. *Neurosurg Focus*. 2014;36(4):E14.
21. Al-Mefty O, Holoubi A, Rifai A, Fox JL. Microsurgical removal of suprasellar meningiomas. *Neurosurgery*. 1985;16(3):364–72.
22. Kim YH, Wang KC, Phi JH, Kim SK. Endoscopic Endonasal approach for Suprasellar lesions in children: complications and prevention. *J Korean Neurosurg Soc*. 2017;60(3):315–21.
23. Koutourousiou M, Fernandez-Miranda JC, Stefko ST, Wang EW, Snyderman CH, Gardner PA. Endoscopic endonasal surgery for suprasellar meningiomas: experience with 75 patients. *J Neurosurg*. 2014;120(6):1326–39.
24. Turel MK, Tsermoulas G, Reddy D, Andrade-Barazarte H, Zadeh G, Gentili F. Endonasal endoscopic transphenoidal excision of tuberculum sellae meningiomas: a systematic review. *J Neurosurg Sci*. 2016;60(4):463–75.
25. Hershey BL. Suprasellar masses: diagnosis and differential diagnosis. *Semin Ultrasound CT MR*. 1993;14(3):215–31.
26. Sahin N, Melhem ER, Wang S, et al. Advanced MR imaging techniques in the evaluation of nonenhancing gliomas: perfusion-weighted imaging compared with proton magnetic resonance spectroscopy and tumor grade. *Neuroradiol J*. 2013;26(5):531–41.
27. Direksunthorn T, Chawalparit O, Sangruchi T, et al. Diagnostic performance of perfusion MRI in differentiating low-grade and high-grade gliomas: advanced MRI in glioma, a Siriraj project. *J Med Assoc Thai*. 2013;96(9):1183–90.
28. Filss CP, Galldiks N, Stoffels G, et al. Comparison of 18F-FET PET and perfusion-weighted MR imaging: a PET/MR imaging hybrid study in patients with brain tumors. *J Nucl Med*. 2014;55(4):540–5.
29. Rossi Espagnet MC, Romano A, Mancuso V, et al. Multiparametric evaluation of low grade gliomas at follow-up: comparison between diffusion and perfusion MR with (18) F-FDOPA PET. *Br J Radiol*. 2016;89(1066):20160476.
30. Zhao S, Kuge Y, Mochizuki T, et al. Biologic correlates of intratumoral heterogeneity in 18F-FDG distribution with regional expression of glucose transporters and hexokinase-II in experimental tumor. *J Nucl Med*. 2005;46(4):675–82.
31. Filss CP, Ciccone F, Shah NJ, Galldiks N, Langen KJ. Amino acid PET and MR perfusion imaging in brain tumours. *Clin Transl Imaging*. 2017;5(3):209–23.
32. Xiangsong Z, Weian C. Differentiation of recurrent astrocytoma from radiation necrosis: a pilot study with 13N-NH3 PET. *J Neuro-Oncol*. 2007;82(3):305–11.
33. Shi X, Zhang X, Yi C, Wang X, Chen Z, Zhang B. The combination of 13N-ammonia and 18F-FDG in predicting primary central nervous system lymphomas in immunocompetent patients. *Clin Nucl Med*. 2013;38(2):98–102.
34. Bergström M, Muhr C, Lundberg PO, Långström B. PET as a tool in the clinical evaluation of pituitary adenomas. *J Nucl Med*. 1991;32(4):610–5.
35. Hyun SH, Choi JY, Lee KH, Choe YS, Kim BT. Incidental focal 18F-FDG uptake in the pituitary gland: clinical significance and differential diagnostic criteria. *J Nucl Med*. 2011;52(4):547–50.
36. De Souza B, Brunetti A, Fulham MJ, et al. Pituitary microadenomas: a PET study. *Radiology*. 1990;177(1):39–44.
37. Ju H, Zhou J, Pan Y, Lv J, Zhang Y. Evaluation of pituitary uptake incidentally identified on 18F-FDG PET/CT scan. *Oncotarget*. 2017;8(33):55544–9.
38. Cooper AJ. 13N as a tracer for studying glutamate metabolism. *Neurochem Int*. 2011;59(4):456–64.
39. Boksha IS, Tereshkina EB, Burbaeva GS. Glutamine synthetase and glutamine synthetase-like protein from human brain: purification and comparative characterization. *J Neurochem*. 2000;75(6):2574–82.
40. Ott P, Larsen FS. Blood-brain barrier permeability to ammonia in liver failure: a critical reappraisal. *Neurochem Int*. 2004;44(4):185–98.
41. Phelps ME, Hoffman EJ, Coleman RE, et al. Tomographic images of blood pool and perfusion in brain and heart. *J Nucl Med*. 1976;17(7):603–12.
42. Phelps ME, Huang SC, Hoffman EJ, Selin C, Kuhl DE. Cerebral extraction of N-13 ammonia: its dependence on cerebral blood flow and capillary permeability – surface area product. *Stroke*. 1981;12(5):607–19.
43. DeBerardinis RJ, Cheng T. Q's next: the diverse functions of glutamine in metabolism, cell biology and cancer. *Oncogene*. 2010;29(3):313–24.
44. He Q, Shi X, Zhang L, Yi C, Zhang X, Zhang X. De novo glutamine synthesis: importance for the proliferation of Glioma cells and potentials for its detection with 13N-Ammonia. *Mol Imaging*. 2016;15:15/0/1536012116645440.
45. Shi X, Zhang X, Yi C, Liu Y, He Q. [¹³N] Ammonia positron emission tomographic/computed tomographic imaging targeting glutamine synthetase expression in prostate cancer. *Mol Imaging*. 2014;13(13):1–10.
46. McCormick D, McQuaid S, McCusker C, Allen IV. A study of glutamine synthetase in normal human brain and intracranial tumours. *Neuropathol Appl Neurobiol*. 1990;16(3):205–11.
47. Spampinato MV, Smith JK, Kwock L, et al. Cerebral blood volume measurements and proton MR spectroscopy in grading of oligodendroglial tumors. *AJR Am J Roentgenol*. 2007;188(1):204–12.
48. Kung HN, Marks JR, Chi JT. Glutamine synthetase is a genetic determinant of cell type-specific glutamine independence in breast epithelia. *PLoS Genet*. 2011;7(8):e1002229.
49. Labow BI, Souba WW, Abcouwer SF. Mechanisms governing the expression of the enzymes of glutamine metabolism—glutaminase and glutamine synthetase. *J Nutr*. 2001;131(9 Suppl):2467S–74S discussion 2486S–7S.
50. Shirasawa N, Yamanouchi H. Glucocorticoids induce glutamine synthetase in folliculostellate cells of rat pituitary glands in vivo and in vitro. *J Anat*. 1999;194(Pt 4):567–77.
51. Xiangsong Z, Dianchao Y, Anwu T. Dynamic 13N-ammonia PET: a new imaging method to diagnose hypopituitarism. *J Nucl Med*. 2005;46(1):44–7.

Publisher's Note

Springer Nature remains neutral with regard to jurisdictional claims in published maps and institutional affiliations.

Ready to submit your research? Choose BMC and benefit from:

- fast, convenient online submission
- thorough peer review by experienced researchers in your field
- rapid publication on acceptance
- support for research data, including large and complex data types
- gold Open Access which fosters wider collaboration and increased citations
- maximum visibility for your research: over 100M website views per year

At BMC, research is always in progress.

Learn more [biomedcentral.com/submissions](https://www.biomedcentral.com/submissions)

